Research Square

Preprints are preliminary reports that have not undergone peer review.
They should not be considered conclusive, used to inform clinical practice,
or referenced by the media as validated information.

Valorization of Pomelo Peel into a Carboxyl-Rich Adsorbent for Charge-Selective Removal of Cationic Dyes

Linlin Du

linlindu0916@163.com

Henan University of Engineering

Jiaxing Jiang

Henan University of Engineering

Dayong Xie

Henan Tongtai Textile Co., Ltd

Yingbo Zhang

Henan University of Engineering

Bing Niu

Henan University of Engineering

Sisi Ma

Henan University of Engineering

Wenying Shi

Henan University of Engineering

Research Article

Keywords: Pomelo peel, Biomass valorization, Carboxyl functionalization, Cationic dye adsorption

Posted Date: August 3rd, 2026

DOI: https://doi.org/10.21203/rs.3.rs-10078893/v1

License: This work is licensed under a Creative Commons Attribution 4.0 International License. Read Full License

Additional Declarations: No competing interests reported.

Abstract

Efficient treatment of multicomponent dye effluents requires low-cost adsorbents that combine high adsorption capacity, selectivity, and reusability. In this study, a carboxyl-functionalized pomelo peel biosorbent (CPP) was prepared through alkali treatment, oxidative bleaching and esterification grafting. The modification introduced abundant carboxylate groups, converted the compact biomass matrix into a porous nanoparticulate architecture, increased the specific surface area from 8.19 to 17.41 $m^2 \cdot g^{-1}$ and produced a superhydrophilic, negatively charged surface. CPP preferentially adsorbed cationic dyes, achieving removal efficiencies exceeding 90% for methylene blue (MB) and methyl violet (MV), while exhibiting limited affinity for anionic dyes. The maximum adsorption capacities estimated using the Langmuir model were 954.20 $mg \cdot g^{-1}$ for MB and 1170.96 $mg \cdot g^{-1}$ for MV. The adsorption process followed the pseudo-second-order kinetic model and was thermodynamically spontaneous and endothermic. Competitive adsorption and column separation experiments further demonstrated the effective separation of cationic dyes from mixed-dye systems. After six adsorption-desorption cycles, CPP retained adsorption capacities of 566.37 $mg \cdot g^{-1}$ for MB and 809.10 $mg \cdot g^{-1}$ for MV. Mechanistic analyses indicated that electrostatic attraction was the predominant driving force, with hydrogen bonding providing an additional contribution. These findings demonstrate the potential of CPP as a reusable biosorbent for the selective treatment of dye-contaminated water.

Introduction

The rapid development of textile dyeing and printing industries has led to the discharge of large volumes of dye-containing wastewater, posing serious risks to aquatic ecosystems and human health. Synthetic dyes usually possess complex aromatic structures, high chromaticity, and strong resistance to biodegradation, making them difficult to remove by conventional biological treatment processes[1–3]. Among them, cationic dyes such as methylene blue (MB) and methyl violet (MV) are widely used in textile, leather, paper, and printing industries. Their high water solubility and strong color intensity can cause persistent contamination even at low concentrations[4–7]. Therefore, the development of efficient, low-cost, and selective treatment technologies for cationic dye wastewater is of considerable environmental importance.

Adsorption is regarded as one of the most practical methods for dye removal because of its operational simplicity, high efficiency, low energy consumption, and broad applicability. Various adsorbents, including activated carbon, clay minerals, metal–organic frameworks, carbon-based nanomaterials, and polymeric materials, have been investigated for dye adsorption[8–12]. Dahlan et al.[13] fabricated industrial waste-modified metal-organic frameworks (MOF-5) adsorbents, among which MOF-5@RHA900 was applied to efficiently adsorb brilliant green (BG) dye with a maximum adsorption capacity of 30.22 $mg \cdot g^{-1}$. And Hussain et al.[14] synthesized a novel Myrrh/GO-TiO_2 nano-adsorbent for the removal of methyl red, with the maximum adsorption capacity of 775.19 $mg \cdot g^{-1}$. Li et al.[15] prepared FGA-PC composite adsorbents composed of foaming gelatin aerogel and porous carbon via 3D printing technology, which achieved highly selective adsorption of the anionic dyes Orange-G (OG) and Methyl-Orange (MO) with prominent removal efficiencies. However, many of these materials suffer from high preparation costs, complicated synthesis procedures, limited regenerability, or insufficient selectivity in multicomponent wastewater systems. In actual dyeing wastewater, anionic and cationic dyes, inorganic salts, and other dissolved species often coexist, which can seriously interfere with adsorption performance[16–20]. Thus, adsorbents with high capacity, good selectivity, salt tolerance, and reusability are highly desirable for practical wastewater treatment.

Biomass-derived adsorbents have attracted increasing attention owing to their abundant availability, low cost, biodegradability, and environmental compatibility. Agricultural and food-processing wastes contain cellulose, hemicellulose, lignin, pectin, and other oxygen-rich components, which provide abundant hydroxyl, carboxyl, and ether groups for further functional modification[21–25]. Pomelo peel is a typical fruit-processing waste with a naturally porous lignocellulosic structure and rich surface functional groups. Argun et al.[26] adopted pomelo peel as a low-cost and abundant adsorbent to remove reactive blue 114 dye from water with a maximum adsorption capacity of 16 $mg \cdot g^{-1}$. However, unmodified pomelo peel adsorbents suffer from a dense biomass matrix, low specific surface area, poor dispersion, and insufficient density of effective adsorption sites, which result in low adsorption capacity and thus limit their practical applications. Therefore, rational chemical modification is required to improve its interfacial activity and adsorption performance.

Carboxyl functionalization is an effective strategy for enhancing the adsorption selectivity of biomass materials toward cationic dyes. Carboxyl groups can dissociate in aqueous media to form negatively charged carboxylate sites, which interact strongly with positively charged dye molecules through electrostatic attraction[27–29]. Meanwhile, residual hydroxyl and carboxyl groups on the biomass skeleton may further stabilize dye molecules through hydrogen bonding. Compared with unmodified biomass, carboxyl-functionalized biomass adsorbents are expected to exhibit improved hydrophilicity, stronger negative surface charge, more accessible active sites, and enhanced affinity toward cationic pollutants. Nevertheless, achieving high adsorption capacity, selectivity, and cyclic stability simultaneously remains challenging, particularly under complex water conditions and continuous-flow operation.

In this work, a carboxyl-functionalized pomelo-peel biosorbent, denoted as CPP, was prepared through alkaline treatment, oxidative bleaching, and esterification grafting. The modification process introduced abundant carboxylate groups onto the pomelo-peel matrix and reconstructed the native compact biomass into a porous nanoparticulate structure. The morphology, surface chemistry, pore structure, wettability, thermal stability, and surface charge of the adsorbent were systematically characterized. The selective adsorption performance of CPP toward representative cationic dyes, including MB and MV, was evaluated in comparison with anionic dyes such as methyl orange and tartrazine. Adsorption kinetics, isotherms, and thermodynamics were analyzed to clarify the adsorption behavior and interfacial mechanism. In addition, competitive adsorption, salt-interference, regeneration, and fixed-bed column experiments were conducted to assess the practical applicability of CPP in complex dyeing wastewater systems. This study provides a simple and sustainable route for converting pomelo-peel waste into a high-performance selective biosorbent for efficient removal of cationic dyes from water.

Experimental Section

2.1. Materials and Characterization

Fresh pomelo peel was obtained from a local fresh-produce market. Absolute ethanol, sodium hydroxide, concentrated hydrochloric acid, and acetone were of analytical grade and purchased from Tianjin Fuyu Fine Chemical Co., Ltd. Hydrogen peroxide and *N,N*-dimethylformamide (DMF) were of analytical grade and supplied by Sinopharm Chemical Reagent Co., Ltd. Succinic anhydride and the dye probes methyl orange (MO), methylene blue (MB), tartrazine (TTZ), and methyl violet (MV) were of analytical grade and obtained from Aladdin Reagent Co., Ltd. (Shanghai, China). All chemicals were used as received without further purification.

The morphology of the samples was examined using an S-4800 field-emission scanning electron microscope (Hitachi, JPN). Surface functional groups were analyzed by Fourier-transform infrared spectroscopy using a Nicolet Nexus 470 FTIR spectrometer (Thermo Fisher Scientific, USA). The absorbance of aqueous dye solutions was measured using a UV1600 UV-vis spectrophotometer (Shanghai Mapada Instruments Co., Ltd., CHN). The pH of the adsorption systems was adjusted using a pB-10 precision pH meter (Sartorius Group, GER). The specific surface area and pore structure were determined by low-temperature nitrogen adsorption-desorption analysis using a Tristar 3000 analyzer (Micromeritics Ltd., UK). Thermogravimetric analysis was performed on a TA Q500 thermal analyzer under a high-purity nitrogen atmosphere at a heating rate of 20°C•min^{-1} over the temperature range of 20–800°C (TA Instruments, USA). The zeta potential and hydrodynamic particle-size distribution were measured using a 3000HS nanoparticle size and zeta-potential analyzer (Malvern, UK).

2.2. Preparation of Pomelo-Peel-Based Biosorbents

Fresh pomelo peel was thoroughly rinsed several times with deionized water to remove surface dust, soluble impurities, and loosely attached contaminants. The cleaned peel was dried in a forced-air oven at 80°C for 24 h, pulverized using a multifunctional grinder, and passed through a 100-mesh sieve to obtain a homogeneous pomelo-peel powder.

For alkaline treatment, 100 g of the pretreated pomelo-peel powder was slowly added to 2.0 L of 2.0 mol•L^{-1} NaOH solution in a 5 L three-necked flask. The suspension was stirred at 250 rpm and reacted at 80°C for 4 h. After the reaction, the solid product was separated by vacuum filtration and washed three times with deionized water to remove residual alkali and soluble by-products, affording an alkalized pomelo-peel intermediate.

The alkalized pomelo peel was then transferred to a clean three-necked flask containing 1.0 L of 1.0 mol•L^{-1} NaOH solution. The mixture was heated to 50°C and maintained for 30 min, after which 250 mL of hydrogen peroxide was added dropwise under mechanical stirring at 50 rpm. Oxidative bleaching was conducted at 50°C for 1 h. During the reaction, a small amount of absolute ethanol was continuously added as an antifoaming agent to suppress excessive foaming and maintain homogeneous mixing. The bleached solid was collected by vacuum filtration, washed five times with deionized water to remove residual oxidant, alkali, and trace organic impurities, and then dried at 80°C for 24 h. The obtained pretreated and bleached pomelo-peel material was denoted as PP.

Succinic anhydride functionalization was carried out by dispersing 10.0 g of PP in molten succinic anhydride. The mixture was heated under reflux in an oil bath at 125°C for 6 h. Under these conditions, the surface hydroxyl groups of PP reacted with succinic anhydride through esterification, thereby introducing carboxyl-rich oxygen-containing functional groups onto the pomelo-peel matrix. After the reaction, 100 mL of DMF was added to quench the residual reactive species, and the hot mixture was immediately filtered to recover the solid intermediate. The solid was sequentially washed with acetone, deionized water, and saturated sodium bicarbonate solution to remove unreacted succinic anhydride, esterification by-products, and residual organic species. After washing, the product was vacuum-dried, ground, and sieved to obtain the succinic-anhydride-functionalized pomelo-peel biosorbent, denoted as CPP. The overall preparation procedure for the pomelo-peel-derived adsorbent is illustrated in Figure S1.

2.3. Adsorption Experiments

Batch adsorption experiments were performed using single-component simulated dye wastewater containing MB or MV at predetermined initial concentrations. A specified amount of CPP was added to a sealed conical flask containing a known volume of dye solution. The initial pH was adjusted using dilute HCl or NaOH solution. The flasks were placed in a thermostatic reciprocating shaker and agitated at 200 rpm.

At predetermined time intervals, aliquots were withdrawn and centrifuged to achieve complete solid-liquid separation. The supernatant was diluted, if necessary, to fall within the linear detection range. The residual dye concentration was determined from the absorbance at the corresponding characteristic wavelength using a UV-vis spectrophotometer and calculated according to the Beer-Lambert law.

The effects of key adsorption parameters on the adsorption performance of CPP were systematically investigated, including dye molecular structure, initial solution pH, adsorbent dosage, and coexisting inorganic ions in water, namely Zn^{2+}, Fe^{3+}, Sn^{4+}, Cu^{2+}, Cl^{-}, NO_3^{-}, and SO_4^{2-}. All adsorption experiments were conducted in triplicate with corresponding blank controls, and the results are reported as mean values to minimize random experimental errors.

The dye removal efficiency (*RE*) and equilibrium adsorption capacity (Q_e) were calculated according to Equations (1) and (2), respectively:

$$\mathrm{Q_e} = \frac{(C_0 - C_e)}{m} V$$

1

$$\mathrm{RE} = \frac{(C_0 - C_e)}{C_0} V \times\ 100\backslash\%$$

2

where C_0 and C_e are the initial and equilibrium dye concentrations, respectively, V is the volume of the dye solution, and m is the mass of the adsorbent.

Adsorption kinetics, isotherms, and thermodynamics were analyzed to elucidate the solid–liquid interfacial adsorption mechanism between the modified pomelo-peel adsorbent and dye molecules. These analyses provide information on the time-dependent adsorption behavior, equilibrium distribution between the solid and liquid phases, and interfacial energy changes during adsorption.

Based on the experimental data obtained under the optimized adsorption conditions, the kinetic behavior was fitted using the pseudo-first-order, pseudo-second-order, and intraparticle diffusion models. The equilibrium adsorption data were analyzed using the Langmuir, Freundlich, and Temkin isotherm models. All fittings were performed by nonlinear regression. The most suitable model was selected by comparing the coefficient of determination (R^2) and other fitting parameters. These analyses were used to identify the rate-controlling steps, the distribution characteristics of active adsorption sites, and the thermodynamic driving forces of the adsorption process, thereby providing a theoretical basis for adsorption-mechanism interpretation and process optimization in practical wastewater treatment.

To simulate the complex composition of actual dyeing wastewater, several binary dye systems containing coexisting anionic and cationic dyes were prepared, including TTZ/MV, MO/MB, and MO/MV. A predetermined amount of CPP was added to each binary dye solution, and adsorption was conducted in sealed flasks under constant conditions at room temperature for 2.0 h.

After adsorption, the suspensions were immediately centrifuged to separate the solid and liquid phases. The clarified supernatants were collected and analyzed by full-wavelength UV-vis spectroscopy. Changes in the characteristic absorption peak intensity and peak position before and after adsorption were compared to evaluate the simultaneous adsorption-separation performance of CPP toward coexisting anionic/cationic dyes and to clarify the competitive adsorption behavior at the solid-liquid interface.

2.4. Reusability Experiments

The reusability and cyclic stability of CPP were evaluated through successive adsorption-desorption cycles. Briefly, 200 mg of dried CPP was added to a single-component MB or MV dye solution with a predetermined concentration. Adsorption was performed under the optimized conditions for 2.0 h with constant shaking. After centrifugation, the absorbance of the supernatant was measured at the corresponding characteristic wavelength, and the adsorption capacity of CPP in each cycle was calculated using Eq. (1).

The dye-loaded CPP was regenerated using 0.5 mol•L^{-1} HCl as the desorption solution at a solid-to-liquid ratio of 1:100 g•mL^{-1}. Each desorption step was conducted for 30 min, and the process was repeated three times to ensure sufficient dye removal. After desorption, the regenerated adsorbent was separated, dried at low temperature to constant weight, cooled to room temperature, and reused directly in the next adsorption–desorption cycle. Multiple consecutive cycles were performed to assess the structural stability and long-term reuse potential of CPP.

Results and Discussion

The surface morphologies of PP and CPP are shown in Fig. 1a,b. The unmodified bleached pomelo peel, PP, exhibited a compact, stacked, lamellar aggregate structure with a particle size of approximately 100 μm. Its surface was rough and irregular, with disordered wrinkles and pores. The overall structure was dense, and obvious aggregation of the native biomass matrix was observed, resulting in poor interfacial dispersion and a limited number of exposed adsorption sites available for pollutant binding. After succinic anhydride grafting, the morphology of CPP was markedly reconstructed. The original large lamellar aggregates were effectively disassembled, forming well-dispersed micro-/nanoscale particles. The modified material showed a more regular nanoparticulate morphology with an effective particle size of 100–200 nm, which agreed well with the particle-size distribution results shown in Figure S2. This morphological evolution can be attributed to the successful covalent anchoring of abundant polar carboxyl groups onto the pomelo-peel biomass skeleton during esterification. The steric effects and electrostatic repulsion generated by these highly polar functional groups promoted fibrillation, interlayer exfoliation, and disintegration of the original compact matrix, thereby producing uniformly dispersed functional nanoparticles. Compared with the conventional bulk biomass matrix, the loose and porous nanoparticle-assembled structure of CPP can shorten the diffusion pathway of aqueous dye molecules toward internal active sites, reduce interfacial mass-transfer resistance, and improve the adsorption kinetics at the solid-liquid interface.

Furthermore, the water contact angle of CPP approached 0°, as shown in Figure S3, indicating a superhydrophilic surface. This result confirms that the grafted carboxyl groups significantly improved the surface wettability of CPP[30, 31]. The enhanced hydrophilicity enables rapid dispersion of the adsorbent in aqueous dyeing wastewater and facilitates sufficient contact with pollutant molecules, thereby providing a favorable interfacial and structural basis for efficient adsorption.

Figure 1c shows the FT-IR spectra of PP and CPP, which were used to evaluate the evolution of surface functional groups before and after modification. Both PP and CPP exhibited a broad and intense absorption band at 3436

cm^{-1}, corresponding to the overlapping stretching vibrations of adsorbed water and hydrogen-bonded hydroxyl groups (-OH) on the biomass skeleton. The absorption band near 2921 cm^{-1} was assigned to the symmetric C-H stretching vibrations of aliphatic methylene (-CH_2-) and methyl (-CH_3) groups in the natural cellulose structure of pomelo peel. These bands are typical features of lignocellulosic biomass materials. Compared with PP, CPP displayed a new sharp and intense absorption band at 1724 cm^{-1}, which was attributed to the C = O stretching vibration of carboxyl and ester groups introduced through succinic anhydride grafting. In addition, the characteristic band at 1413 cm^{-1} was associated with the coupled symmetric and asymmetric stretching vibrations of carboxylate groups (-COO^-)[32, 33]. The appearance, shift, and intensity variation of these characteristic FT-IR bands confirm that succinic anhydride was successfully covalently anchored onto the pomelo-peel matrix through esterification, thereby achieving targeted carboxyl functionalization.

The thermal stability of PP and CPP was evaluated by TGA, and the corresponding derivative thermogravimetric curves are shown in Fig. 1d. The main thermal degradation of unmodified PP occurred within 200–400°C, where rapid cleavage and decomposition of the lignocellulosic backbone led to substantial mass loss. At 800°C, the residual char yield of PP was only 15.03 wt%, indicating the relatively poor thermal resistance of the native biomass matrix. After esterification with succinic anhydride, CPP exhibited a higher initial decomposition temperature, and its main degradation region shifted to 260–390°C. Throughout the heating process, CPP retained a higher residual mass than PP at the same temperature. At 800°C, the char yield of CPP increased to 21.49 wt%, demonstrating improved thermal stability and char-forming ability. This enhancement is mainly ascribed to the grafted anhydride-derived functional groups, which can promote in situ crosslinking and cyclization reactions within the pomelo-peel macromolecular framework. Under high-temperature conditions, these reactions facilitate the formation of a compact and continuous carbonaceous protective layer, which inhibits heat and oxygen transfer into the interior of the material and suppresses thermal decomposition of the biomass skeleton. These TGA results are consistent with the FT-IR analysis, further confirming the successful functionalization of CPP.

The pore structure and specific surface area of an adsorbent are critical physicochemical parameters that directly affect adsorption capacity and mass-transfer efficiency at the solid-liquid interface. The nitrogen adsorption-desorption isotherms of PP and CPP are shown in Fig. 1e. The unmodified PP exhibited a compact structure with limited porosity, giving a low specific surface area of 8.19 $m^2 \cdot g^{-1}$. After succinic anhydride-induced carboxylation and structural disintegration, the specific surface area of CPP increased markedly to 17.41 $m^2 \cdot g^{-1}$. The improved pore structure can be attributed to the in situ grafting of highly polar carboxyl groups, which promoted the disassembly of dense native fiber bundles, interlayer exfoliation, and pore formation within the pomelo-peel matrix. This structural evolution agrees well with the SEM observations and DLS particle-size analysis, which revealed fragmentation of the original bulk structure and formation of smaller dispersed particles. The enlarged surface area and hierarchical porous structure expose more accessible adsorption sites and shorten the diffusion pathway of dye molecules, providing a favorable structural basis for the enhanced adsorption performance of CPP.

Figure 1f presents the zeta potentials of PP and CPP over a pH range of 4.0–10.0, providing insight into the surface charge characteristics before and after modification. For both samples, the absolute value of the zeta potential increased gradually with increasing pH, indicating enhanced surface negativity due to the deprotonation of oxygen-containing functional groups. At the same pH, CPP consistently showed a higher absolute zeta potential than PP, suggesting a stronger negatively charged surface. This result further confirms that succinic anhydride modification effectively introduced abundant dissociable carboxyl groups onto the pomelo-peel matrix. From the perspective of interfacial electrostatic interactions, the strongly negatively charged CPP surface can efficiently capture cationic

dye molecules through electrostatic attraction[34]. This provides a direct electrochemical basis for the superior adsorption potential of CPP toward cationic dyes.

Adsorption Performance

To evaluate the selective adsorption behavior of the adsorbents toward typical pollutants in dyeing wastewater, two cationic dyes, MB and MV, and two anionic dyes, TTZ and MO, were selected as representative target pollutants. The adsorption removal efficiencies of PP and CPP are compared in Figure 2a.

The unmodified PP showed weak adsorption toward all four dyes, with removal efficiencies below 40% and no obvious adsorption selectivity. This indicates that the native biomass matrix has limited broad-spectrum adsorption ability. In contrast, the carboxyl-functionalized CPP exhibited excellent selective removal of the cationic dyes MB and MV, with removal efficiencies above 90% in single-component systems. However, CPP showed much lower removal efficiencies toward the anionic dyes TTZ and MO, indicating pronounced charge-selective adsorption behavior.

This selective adsorption can be rationally explained by interfacial electrostatic interactions. After succinic anhydride grafting, abundant negatively charged carboxylate sites ($-COO^-$) were introduced onto the CPP surface. These sites can strongly interact with positively charged functional groups on cationic dye molecules, thereby enabling efficient dye capture and enrichment. In contrast, the anionic dyes TTZ and MO contain negatively charged sulfonate groups ($-SO_3^-$), which experience strong electrostatic repulsion from the negatively charged CPP surface[35]. This repulsive interaction hinders the approach of anionic dye molecules to the adsorption interface, resulting in low adsorption capacities.

The initial solution pH is a key parameter governing solid-liquid interfacial adsorption because it determines both the speciation of dye molecules and the dissociation state of surface functional groups on the adsorbent. Therefore, the adsorption performance of CPP toward MB and MV was evaluated over a pH range of 4.0-10.0, and the results are shown in Figure 2b.

As the pH increased from weakly acidic to weakly alkaline conditions, the equilibrium adsorption capacity of CPP increased from 204.5 to 670.2 $mg·g^{-1}$ for MB and from 372.5 to 987.2 $mg·g^{-1}$ for MV, indicating a clear positive correlation between pH and adsorption capacity. This trend is consistent with the zeta-potential results, which showed that CPP maintained a negatively charged surface throughout the tested pH range. Under acidic conditions, abundant H^+ ions compete with cationic dye molecules for the limited active adsorption sites on CPP. Meanwhile, protonation of surface carboxylate groups decreases the density of negatively charged $-COO^-$ sites, thereby weakening electrostatic attraction between CPP and the cationic dyes. With increasing pH, the carboxyl groups are progressively deprotonated, leading to a higher surface negative-charge density and reduced competition from H^+. Consequently, electrostatic attraction is enhanced, resulting in improved adsorption of cationic dyes.

Figure 2c shows the effect of initial dye concentration on the removal of MB and MV by CPP. Under standard adsorption conditions at room temperature, when the initial dye concentration increased from 10 to 500 $mg·L^{-1}$, the removal efficiencies of MB and MV decreased by 22.83% and 24.89%, respectively. At low dye concentrations, the abundant available adsorption sites on CPP are sufficient to capture most dye molecules, resulting in high removal efficiency. At higher concentrations, the limited active sites become progressively saturated, leading to a higher

fraction of residual dye molecules in solution and a gradual decrease in removal efficiency. Nevertheless, the adsorption capacity per unit mass of CPP continues to increase as the concentration gradient provides a stronger driving force for dye transfer.

Because practical dyeing wastewater generally contains various soluble inorganic ions that may disturb electrostatic adsorption equilibria, the influence of coexisting ions on the adsorption performance of CPP was further investigated[36]. As shown in Figure 2d, the removal efficiencies of CPP toward MB and MV showed no obvious decrease in the presence of different interfering anions and cations. This result indicates that the salt-interference effect was negligible under the tested conditions. The excellent salt tolerance of CPP can be attributed to the strong and specific electrostatic interaction between the densely distributed negatively charged carboxylate groups on CPP and the positively charged sites of cationic dye molecules. These results demonstrate that the carboxyl-functionalized pomelo-peel adsorbent has good adaptability to complex aqueous environments and shows potential for practical treatment of industrial dyeing wastewater.

Adsorption kinetics directly reflect the rate of pollutant transfer and enrichment at the solid-liquid interface and are important for determining the optimal hydraulic retention time in water-treatment processes. The effect of contact time on the adsorption of MB and MV by CPP was therefore investigated, and the kinetic curves are shown in Figure 3a. The adsorption process can be divided into three stages: rapid uptake, gradual approach to equilibrium, and dynamic equilibrium. During the first 30 min, dye molecules rapidly diffuse across the liquid-film boundary and bind to active sites on the CPP surface under strong electrostatic attraction, resulting in a sharp increase in adsorption capacity. As the available active sites are gradually occupied, the mass-transfer driving force decreases and the adsorption rate slows. After approximately 50 min, the distribution of dye molecules between the solid and liquid phases reaches dynamic equilibrium, and the adsorption capacity remains nearly constant. This rapid adsorption equilibrium is mainly attributed to the strong directional electrostatic interaction between the high-density negatively charged carboxylate sites on CPP and the cationic dye molecules, highlighting the practical advantages of CPP for rapid treatment of dye-containing wastewater and continuous water-treatment processes.

To further clarify the microscopic adsorption mechanism and identify the rate-controlling step, the kinetic data for MB and MV adsorption were fitted using the pseudo-first-order, pseudo-second-order, and intraparticle diffusion models. The fitted curves are shown in Figure 3b and Figure S4, and the corresponding kinetic parameters are summarized in Table 1.

The pseudo-second-order model provided the best fit for the adsorption of both dyes, outperforming the pseudo-first-order and intraparticle diffusion models. The correlation coefficients (R^2) for MB and MV were both close to 0.99, and the calculated equilibrium adsorption capacities agreed well with the experimental values, with negligible deviations. These results indicate that the adsorption of MB and MV onto CPP follows pseudo-second-order kinetics. The rate-controlling step is therefore mainly governed by interfacial interactions between the active functional groups on CPP and dye molecules, including electrostatic binding and possible electron-sharing interactions, rather than by physical pore diffusion. This confirms that the strong electrostatic/chemical coupling between grafted carboxylate groups and cationic dye molecules is the primary driving force responsible for the efficient and selective adsorption of cationic dyes by CPP[37, 38].

Table 1. Kinetic parameters for the adsorption of MV and MB onto CPP.

Dye	$Q_{e\text{-}exp}$ ($mg \cdot g^{-1}$)	Pseudo-Second-Order			Pseudo-First-Order			Intraparticle Diffusion		
		$t/Q_t = 1/K_2Q_e^2 + t/Q_e$			$\ln(Q_e - Q_t) = \ln Q_e - K_1 t$			$Q_t = K_i t^{0.5} + C$		
		$Q_{e\text{-}cal}$ ($mg \cdot g^{-1}$)	K_2 ($g \cdot mg^{-1} \cdot min^{-1}$)	R^2	$Q_{e\text{-}cal}$ ($mg \cdot g^{-1}$)	K_1 (min^{-1})	R^2	K_i	C	R^2
MV	676.31	680.27	0.0002	0.99	368.71	0.035	0.88	42.59	186.07	0.73
MB	1086.03	1092.90	0.0007	0.99	119.10	0.024	0.84	19.48	861.91	0.61

Figure 3c shows the equilibrium adsorption capacities of CPP toward MB and MV at different initial dye concentrations, together with the corresponding nonlinear isotherm fitting curves. As the initial dye concentration increased, the equilibrium adsorption capacity of CPP for both cationic dyes first increased rapidly and then gradually approached a saturation plateau.

This trend can be explained by the balance between dye concentration and available adsorption sites. At low dye concentrations, abundant negatively charged carboxylate sites on the CPP surface remain unoccupied, allowing dye molecules to rapidly bind to accessible active sites. Consequently, the adsorption capacity increases markedly with increasing initial concentration. When the dye concentration exceeds a critical level, the finite interfacial active sites become progressively occupied. As the adsorption surface approaches saturation, the additional mass-transfer driving force becomes less effective, and the increase in adsorption capacity slows until dynamic equilibrium is reached.

To clarify the equilibrium distribution behavior and microscopic adsorption configuration at the solid-liquid interface, the experimental isotherm data were fitted using the Langmuir, Freundlich, and Temkin models. The nonlinear fitting curves are shown in Figure 3d and Figure S5, and the corresponding isotherm parameters are summarized in Table 2.

Among the three models, the Langmuir model provided the best fit for both MB and MV adsorption, with correlation coefficients closer to unity than those obtained from the Freundlich and Temkin models. This result indicates that the adsorption of cationic dyes onto CPP follows a monolayer adsorption mechanism on a relatively homogeneous surface. In this model, dye molecules are uniformly adsorbed onto energetically equivalent active sites, and no significant lateral stacking or interaction between adsorbed dye molecules occurs after surface saturation[39, 40].

Based on the Langmuir model, the theoretical maximum monolayer adsorption capacities of CPP were calculated to be 954.20 mg·g^{-1} for MB and 1170.96 mg·g^{-1} for MV. These results further demonstrate that succinic anhydride-mediated carboxyl functionalization effectively enhances the adsorption performance of the native pomelo-peel biomass matrix and enables efficient, selective removal of typical cationic dyes from dyeing wastewater. This green modification strategy therefore shows promising potential for the controllable preparation of high-performance biomass adsorbents and for practical wastewater-treatment applications.

Table 2. Isotherm parameters for the adsorption of MB and MV on CPP.

Isotherm Model	Parameters	MB	MV
Langmuir: $C_e/Q_e = C_e/Q_m + 1/Q_mK_L$	$Q_m/(mg{\cdot}g^{-1})$	954.20	1170.96
	$K_L/(L{\cdot}mg^{-1})$	0.03	0.12
	R^2	0.99	0.99
Freundlich: $lnQ_e = lnK_F + b_FlnC_e$	$K_F/(mg{\cdot}g^{-1})$	80.64	186.79
	b_F	0.48	0.37
	R^2	0.92	0.86
Temkin: $Q_e = BlnK_T + BlnC_e$	$K_T/(L{\cdot}mg^{-1})$	0.26	1.94
	$B/(KJ^{-2}{\cdot}mol^{-2})$	240.29	195.22
	R^2	0.98	0.95

To further elucidate the interfacial adsorption mechanism of CPP toward the cationic dyes MB and MV from an energetic perspective, temperature-dependent adsorption experiments were performed, and the corresponding thermodynamic parameters were calculated. The results are shown in Figure 4 and Table 3.

The equilibrium adsorption capacities of CPP toward both MB and MV increased gradually with increasing temperature, indicating that moderate heating favored dye uptake at the solid-liquid interface. The equilibrium data obtained at different temperatures were analyzed using the classical van't Hoff equation. A good linear relationship was observed between $\ln(Q_e/C_e)$ and $1/T$, with correlation coefficients (R^2) of approximately 0.99 for both dye systems. This confirms the reliability of the thermodynamic fitting and supports the quantitative calculation of the thermodynamic parameters.

The calculated thermodynamic parameters provide insight into the energetic nature of the adsorption process. The positive standard enthalpy change (ΔH^0) indicates that the adsorption of MB and MV onto CPP is endothermic. Increasing temperature can supply additional activation energy, reduce the diffusion and mass-transfer barriers, and strengthen the interfacial interactions between dye molecules and active sites, thereby enhancing the adsorption capacity.

The standard Gibbs free energy change (ΔG^0) remained negative over the entire temperature range, confirming that the adsorption process is spontaneous. Moreover, as the temperature increased from 25 to 45 $^{\circ}$C, the absolute value of ΔG^0 gradually increased, suggesting that higher temperature enhances the spontaneity of adsorption and strengthens the driving force for dye transfer from the liquid phase to the CPP surface.

The positive standard entropy change (ΔS^0) indicates increased randomness at the solid–liquid interface after adsorption. This may arise from the redistribution of water molecules, counterions, and dye molecules during interfacial binding, which increases the overall disorder of the adsorption system[41].

Overall, the thermodynamic results are consistent with the temperature-dependent adsorption behavior. Moderate heating promotes CPP adsorption through several cooperative effects: it supplies the activation energy required for

the endothermic adsorption process, enhances the spontaneity of interfacial binding, facilitates dye diffusion and mass transfer, and increases interfacial disorder. These effects collectively contribute to the efficient capture of MB and MV cationic dyes by CPP.

Table 3 Thermodynamic parameters for MB and MV adsorption by CPP

Dye	ΔH^0	ΔS^0	ΔG^0 (kJ·mol^{-1})		
	(KJ·mol^{-1})	(J·mol^{-1}·K^{-1})	298K	308K	318K
MB	10.72	44.56	-2.56	-3.01	-3.45
MV	46.72	177.25	-6.11	-7.88	-9.65

To systematically evaluate the engineering applicability of CPP for continuous-flow treatment of dyeing wastewater, dynamic adsorption experiments were performed using a laboratory-made fixed-bed column. A single-component MB solution and a binary dye mixture containing MB and TTZ were used to assess the continuous decolorization and enrichment performance of CPP. The breakthrough behavior and visual decolorization results are shown in Figure 5 and Figure S6.

The fixed-bed column experiments showed that, when a concentrated cationic MB solution passed through the CPP-packed column, the effluent became clear and colorless, indicating efficient in situ removal of MB. For the binary MB/TTZ dye mixture, the cationic MB component was selectively retained by the CPP adsorbent bed, whereas the intrinsic color of the anionic TTZ remained in the effluent. This result demonstrates that CPP can selectively separate and remove cationic dyes from multicomponent dye systems.

These dynamic-flow experiments directly confirm that the CPP-packed fixed bed can recognize and capture cationic dye molecules with high selectivity. More importantly, CPP retained its selective decolorization ability under continuous-flow conditions, indicating its promising applicability for integrated and continuous treatment of practical dyeing wastewater.

High selectivity is a key prerequisite for the advanced industrial application of functional adsorbents, and the development of high-performance selective adsorption materials has become a major focus in the field of water pollution control. Based on batch competitive adsorption experiments in multicomponent systems, the selective recognition and adsorption performance of CPP toward typical mixed anionic/cationic dye systems was further quantitatively evaluated. The photographic images of the binary dye mixtures before and after adsorption, together with the corresponding full-scan UV-vis spectra, are presented in Figure 6.

Comparison of the solution color before and after adsorption, as well as the evolution of the characteristic UV-vis absorption peaks, showed that after equilibrium adsorption by CPP, the characteristic absorption peaks of the cationic dyes MB and MV in the MO/MV, MO/MB, and TTZ/MB binary systems were almost completely extinguished, with their intensities decreasing to nearly baseline levels. In contrast, the characteristic absorption peaks of the anionic dyes MO and TTZ remained essentially unchanged in both shape and intensity. These spectral results were further supported by the photographic observations, which showed that after adsorption the mixed solutions retained only the characteristic color of the anionic dyes, whereas the cationic dyes were almost completely removed.

Taken together, the spectroscopic and visual results clearly demonstrate that carboxyl-functionalized CPP exhibits excellent selectivity toward the cationic dyes MB and MV in aqueous media, together with strong resistance to interference from coexisting anionic dyes.

The recyclability and long-term structural stability of an adsorbent are critical techno-economic factors for reducing operating costs in practical water treatment, improving solid-waste valorization, and promoting large-scale engineering application. To evaluate the long-term reusability of CPP, 0.5 mol·L^{-1} HCl, a low-cost and readily available eluent, was used to regenerate MB- and MV-loaded CPP through stepwise offline desorption. The adsorption-desorption cycling results are shown in Figure 7.

As the number of adsorption-desorption cycles increased, the equilibrium adsorption capacities of CPP toward both cationic dyes decreased only slightly. No abrupt performance deterioration, framework collapse, or structural failure was observed. Even after six consecutive adsorption-regeneration cycles, CPP retained high equilibrium adsorption capacities of 566.37 mg·g^{-1} for MB and 809.10 mg·g^{-1} for MV, indicating excellent retention of adsorption performance.

These recycling results confirm that the carboxyl-functionalized interfacial structure formed by succinic anhydride grafting has high physicochemical stability. Under repeated adsorption and acid-regeneration conditions, the CPP framework remained stable, and the loss of active sites was limited. Therefore, CPP exhibits good fatigue resistance, efficient regeneration capability, and strong reuse potential.

Overall, these findings provide experimental evidence for the long-term and cost-effective application of modified biomass adsorbents in scalable treatment of dyeing wastewater, highlighting the practical advantages of CPP in low-cost and environmentally sustainable water purification.

3.10. Adsorption Mechanism

To elucidate the selective adsorption mechanism of CPP toward cationic dyes from the perspectives of elemental composition and interfacial chemical interactions, energy-dispersive X-ray spectroscopy (EDS) and Fourier-transform infrared spectroscopy (FTIR) were performed on CPP before and after adsorption.

Figure 8a shows the elemental distribution and relative composition of CPP before and after MB adsorption. The pristine CPP mainly contained the intrinsic biomass elements C and O, with no detectable signals from other elements. After saturated adsorption of MB, a new sulfur signal was observed on the CPP surface, with a sulfur content of 5.77 wt%. Considering the molecular structure of MB, this sulfur signal can be attributed to MB molecules immobilized on the CPP surface. This result provides direct elemental evidence that MB was successfully captured and enriched by the functionalized CPP interface.

FT-IR analysis was further used to identify the interfacial interactions between CPP and dye molecules. As shown in Figure 8b, compared with pristine CPP, the MB-loaded CPP sample displayed a new absorption band at 1570 cm^{-1}, which is assigned to the stretching vibration of the aromatic heterocyclic conjugated framework of MB. This characteristic MB fingerprint band further confirms that MB molecules were firmly anchored onto the porous CPP surface after adsorption.

Based on the morphology, zeta-potential, thermodynamic, EDS, and FTIR results, the adsorption mechanism of CPP toward the cationic dyes MB and MV can be proposed as follows. The dominant driving force is the strong electrostatic attraction between the high-density negatively charged carboxylate sites (-COO^-) on CPP and the

positively charged functional groups of the cationic dye molecules. In addition, residual hydroxyl and carboxyl groups on the pomelo-peel biomass skeleton may form hydrogen bonds with heteroatom-containing sites in the dye molecules, further stabilizing the adsorbed species at the solid-liquid interface. These cooperative interactions contribute to the efficient and selective enrichment of cationic dyes by CPP. The proposed adsorption pathway and interfacial mechanism are illustrated in Figure S1.

Conclusions

A carboxyl-functionalized pomelo peel adsorbent (CPP) was prepared through succinic anhydride-mediated esterification for the selective removal of cationic dyes. The modification introduced abundant carboxyl groups, increased surface area and negative charge, and improved the porosity, hydrophilicity, and thermal stability of the biomass. CPP showed strong selectivity toward methylene blue (MB) and methyl violet (MV), with maximum Langmuir adsorption capacities of 954.20 and 1170.96 $mg \cdot g^{-1}$, respectively, while exhibiting limited adsorption of anionic dyes. The adsorption process followed the pseudo-second-order kinetic model and was spontaneous and endothermic. Competitive adsorption and column separation experiments confirmed efficient separation of cationic dyes from mixed-dye systems. CPP also showed good salt tolerance and regeneration cycles. Electrostatic attraction between negatively charged carboxylate groups and cationic dye molecules was the main adsorption mechanism, with hydrogen bonding providing an additional contribution. These results demonstrate that CPP is a promising low-cost and sustainable adsorbent for the selective treatment of cationic dye-contaminated wastewater.

Declarations

Author contributions

L. Du: Writing-review and editing, original draft, Data curation, Conceptualization, Funding acquisition. **J. Jiang**: Synthesis and characterization, Adsorption experiments. **D. Xie:** Methodology, Formal analysis. **Y. Zhang**: Investigation, Validation. **B. Niu**: Visualization, Supervision, Data curation, Conceptualization, Funding acquisition. **S. Ma:** Mechanism analysis, Conceptualization. **W. Shi**: Data analysis, review and editing. All authors have read and agreed to the published version of the manuscript.

Acknowledgements

This work was supported by the Joint Fund of Henan Provincial Science and Technology Research and Development Program (No. 252103810081), the Natural Science Foundation of Henan Province (No. 262300421916) and the China National University Student Innovation and Entrepreneurship Development Program (202511517013).

Conflict of interests

There are no conflicts to declare.

Data Availability Statement

The data that support the findings of this study are available on request from the corresponding author.

References

1. Katheresan, V., Kansedo, J., & Lau, S. Y. (2018). Efficiency of various recent wastewater dye removal methods: A review. *Journal of environmental chemical engineering, 6(4)*, 4676-4697. https://doi.org/10.1016/j.jece.2018.06.060
2. Lu, T., Zhang, Q., & Yao, S. (2017). Removal of dyes from wastewater by growing fungal pellets in a semi-continuous mod. *Frontiers of Chemical Science and Engineering*, *11(3)*, 338-345. https://doi.org/10.1007/s11705-017-1644-0
3. Praveen, S., Jegan, J., Pushpa, B. T., Gokulan, R., & Bulgariu, L. (2022). Biochar for removal of dyes in contaminated water: an overview. *Biochar*, *4*, Article 10. https://doi.org/10.1007/s42773-022-00131-8
4. Jaberi, H., Emami, E., & Mousazadeh, M. H. (2022). CDs/HMS for removal of MB dye with highly adsorption capacity: isotherm, kinetic, and thermodynamic study. *International Journal of Environmental Science and Technology*, *19*, 5167-5180. https://doi.org/10.1007/s13762-021-03723-2
5. Barros, C. G. K. G., Duarte, L. J. N., Melo, R. P. F., Lopes, F. W. B., & Neto, E. L. B. (2022). Ionic dye removal using solvent-assisted ionic micellar flocculation. *Journal of Polymers and the Environment*, *30(6)*, 2534-2546. https://doi.org/10.1007/s10924-021-02360-7
6. Adenan, N. H., Lim, Y. Y., & Ting, A. S. Y. (2022). Removal of triphenylmethane dyes by Streptomyces bacillaris: A study on decolorization, enzymatic reactions and toxicity of treated dye solutions. *Journal of environmental management*, *318*, Article 115520. https://doi.org/10.1016/j.jenvman.2022.115520
7. Boushehrian, M. M., Esmaeili, H., & Foroutan, R. (2020). Ultrasonic assisted synthesis of Kaolin/$CuFe_2O_4$ nanocomposite for removing cationic dyes from aqueous media. *Journal of Environmental Chemical Engineering*, *8(4)*, Article 103869. https://doi.org/10.1016/j.jece.2020.103869
8. Sriram, G., Bendre, A., Mariappan, E., Altalhi, T., Kigga, M., Ching, Y. C., Jung, H. Y., Bhaduri, B., & Kurkuri, M. (2022). Recent trends in the application of metal-organic frameworks (MOFs) for the removal of toxic dyes and their removal mechanism-a review. *Sustainable Materials and Technologies*, *31*, Article 00378. https://doi.org/10.1016/j.susmat.2021.e00378
9. Tayeb, B., Lahcene, S., Yazid, D., Mohammed, M., Soltani, T., Alsaeedi, H., Cornu, D., Bechelany, M., & Barhoum, A. (2026). Dye removal by adsorption using Fe_3O_4 and ε-Fe_2O_3-based kaolinite nanocomposites synthesized with an apricot kernels shell extract. *Applied Water Science*, *16*, Article 66. https://doi.org/10.1007/s13201-026-02752-x
10. Kumar, N., Pandey, A., & Sharma, Y. C. (2023). A review on sustainable mesoporous activated carbon as adsorbent for efficient removal of hazardous dyes from industrial wastewater. *Journal of Water Process Engineering*, *54,* Article 104054. https://doi.org/10.1016/j.jwpe.2023.104054
11. Thakur, A., Kumar, A., & Singh, A. (2024). Adsorptive removal of heavy metals, dyes, and pharmaceuticals: Carbon-based nanomaterials in focus. *Carbon*, *217*, Article 118621. https://doi.org/10.1016/j.carbon.2023.118621
12. Choi, B. H., Jung, K. W., Choi, J. W., Lee, S. H., Lee, Y. J., & Ahn, K. H. (2017). Facile one-pot synthesis of imidazole-functionalized poly-(vinylbenzyl chloride) and its study on the applicability of synthetic dye removal from aqueous system. *Journal of cleaner production*, *168*, 510-518. https://doi.org/10.1016/j.jclepro.2017.09.074
13. Dahlan, I., Obi, C. C., Razaman, N. S., Razaman, N. S., & Hasan, H. Y. A. (2024). Adsorptive decolorization of brilliant green dye in aqueous media using various modified MOF-5 adsorbents. *Groundwater for Sustainable Development*, *26*, Article 101228. https://doi.org/10.1016/j.gsd.2024.101228

14. Hussain, M., Hussaini, S. S., Shariq, M., Alshehri, E. M., AlRisi, S., AlNoufali, M., AlSaidi H., AlYahmadi, I. Z., & Khatab, A. (2026). Efficient adsorptive removal of methyl red dye using a novel myrrh/GO-TiO_2 Nano-adsorbent: Synthesis, characterization, and adsorption studies. *Diamond and Related Materials*, *161*, Article 113131. https://doi.org/10.1016/j.diamond.2025.113131
15. Li, J. X., Zhao, Y. J., Yu, Y. F., Huang, Q. Q., Qi S. C., Liu, X. Q., & Sun, L. B. (2025). The selective adsorption of anionic dyes over 3D printing composite sorbents of aerogel and porous carbon. *Separation and Purification Technology*, *360*, Article 130945. https://doi.org/10.1016/j.seppur.2024.130945
16. Wan, H., Zhu, X., Wang, J., Cao, F., Zhang, Y., Yao, Z., Wang, S., Bhattacharyya, D., & Tang, K. (2025). Adsorptive nanofibrous membranes for bidirectional removal of cationic and anionic dyes. *Separation and Purification Technology*, *361*, Article 131515. https://doi.org/10.1016/j.seppur.2025.131515
17. Hou, J., Yu, Z., Chen, Z., Jiang, J., Song, Y., Tang, X., & Wang, J. (2025). Fabrication of photothermal membranes with high-efficiency oil-water separation capabilities: Applicable for oil-in-water emulsions, dyes, and metal salt ions. *Langmuir*, *41(34)*, 23050-23063. https://doi.org/10.1021/acs.langmuir.5c02730
18. Gul, S., Afsar, S., Raza, N., Gul, H., Khezami, L., Almufarij, R., & Hussain, S. N. (2024). Efficient adsorptive removal of textile dye neutral red in environmental samples using white clover stem powder. *Biomass Conversion and Biorefinery*, *14(24)*, 31079-31092. https://doi.org/10.1007/s13399-023-04770-0
19. Nagendraprasad, G., Reddy, K. A., Das, C., & Karan, S. (2025). Atomistic insights into high-performance polyimine-based membranes for selective dye rejection and salt permeation in nanofiltration. *Chemical Engineering Science*, *311*, Article 121569. https://doi.org/10.1016/j.ces.2025.121569
20. Li, J., Gong, J. L., Zeng, G. M., Zhang, P., Song, B., Cao, W. C., Liu H. Y., & Huan, S. Y. (2018). Zirconium-based metal organic frameworks loaded on polyurethane foam membrane for simultaneous removal of dyes with different charges. *Journal of colloid and interface science*, *527*, 267-279. https://doi.org/10.1016/j.jcis.2018.05.028
21. Amalina, F., Abd Razak, A. S., Krishnan, S., Zularisam, A. W., & Nasrullah, M. (2022). A review of eco-sustainable techniques for the removal of Rhodamine B dye utilizing biomass residue adsorbents. *Physics and Chemistry of the Earth, Parts A/B/C*, *128*, Article 103267. https://doi.org/10.1016/j.pce.2022.103267
22. Yadav, M., Singh, N., Annu, Khan, S. A., Raorane, C. J., & Shin, D. Kil. (2024). Recent advances in utilizing lignocellulosic biomass materials as adsorbents for textile dye removal: a comprehensive review. *Polymers*, *16(17)*, Article 2417. https://doi.org/10.3390/polym16172417
23. Mishra, S., Cheng, L., & Maiti, A. (2021). The utilization of agro-biomass/byproducts for effective bio-removal of dyes from dyeing wastewater: A comprehensive review. *Journal of Environmental Chemical Engineering*, *9(1)*, Article 104901. https://doi.org/10.1016/j.jece.2020.104901
24. Liu, Z., Khan, T. A., Islam, M. A., & Tabrez, U. (2022). A review on the treatment of dyes in printing and dyeing wastewater by plant biomass carbon. *Bioresource Technology*, *354*, Article 127168. https://doi.org/10.1016/j.biortech.2022.127168
25. Sarkar, P., & Dey, A. (2021). Phycoremediation-an emerging technique for dye abatement: an overview. *Process Safety and Environmental Protection*, *147*, 214-225. https://doi.org/10.1016/j.psep.2020.09.031
26. Argun, M. E., Güclü, D., & Karatas, M. (2014). Adsorption of Reactive Blue 114 dye by using a new adsorbent: Pomelo peel. *Journal of Industrial and Engineering Chemistry*, *20(3)*, 1079-1084. https://doi.org/10.1016/j.jiec.2013.06.045
27. Li, Y., Yang, C. X., Qian, H. L., Zhao, X., & Yan, X. P. (2019). Carboxyl-functionalized covalent organic frameworks for the adsorption and removal of triphenylmethane dyes. *ACS Applied Nano Materials*, *2(11),* 7290-7298.

https://doi.org/10.1021/acsanm.9b01781

28. Zhang, S., Dai, F., Ke, Z., Wang, Q., Chen, C., Qian, G., & Yu, Y. A novel porous hollow carboxyl-polysulfone microsphere for selective removal of cationic dyes. *Chemosphere*, *289*, Article 133205. https://doi.org/10.1016/j.chemosphere.2021.133205
29. Xiao, Z., Zhou, J., Fan, L., Li, Y., He, Y., Wang, Y., & Li, L. (2021). Controllable preparation of Cu-MOF-coated carboxyl filter paper for simultaneous removal of organic dye and metal ions. *Industrial & Engineering Chemistry Research*, *60(19)*, 7311-7319. https://doi.org/10.1021/acs.iecr.1c00140
30. Xiang, T., Xie, Y., Wang, R., Wu, M. B., Sun, S. D., & Zhao, C. S. (2014). Facile chemical modification of polysulfone membrane with improved hydrophilicity and blood compatibility. *Materials Letters*, *137*, 192-195. https://doi.org/10.1016/j.matlet.2014.09.037
31. Shao, Y., Jia, W., Qin, G., Jiang, X., & Xu, Z. (2025). Carboxyl-functionalized BODIPY and Aza-BODIPY dyes: Synthetic strategies and emerging applications. *Coordination Chemistry Reviews*, *543*, Article 216944. https://doi.org/10.1016/j.ccr.2025.216944
32. Moradian, M., Alam, M. N., & Van, T. G. M. (2021). Influence of carboxyl charge density on properties of extruded cellulose films. *Industrial & Engineering Chemistry Research*, *60(38)*, 13756-13763. https://doi.org/10.1021/acs.iecr.1c01716
33. Lin, H., Chen, K., Du, L., Gao, P., Zheng, J., Liu, Y., & Ma, L. (2022). Efficient and selective adsorption of methylene blue and methyl violet dyes by yellow passion fruit peel. *Environmental technology*, *43(23)*, 3519-3530. https://doi.org/10.1080/09593330.2021.1924288
34. Tafese, B. N., Ganesh, T., Solomon, A., Sundararaju, B., Garg, N., & Alebachew, B. (2023). Efficient adsorptive removal of methylene blue dye from aqueous solution using eragrostis teff biomass-derived nitrogen and phosphorus-codoped carbon quantum dots. *Langmuir*, *40(1)*, 72-83. https://doi.org/10.1021/acs.langmuir.3c01813
35. Liu, M., Zheng, J., Wang, L., Hu, Z., Lan, S., Rao, W., Liu, Y., Xie, Y., & Yu, C. (2022). Ultrafast and selective adsorption of anionic dyes with amine-functionalized glucose-based adsorbents. *Journal of Molecular Structure*, *1263*, Article 133150. https://doi.org/10.1016/j.molstruc.2022.133150
36. Zhuo, G. H., Xue, D. X., Huang, L. F., Wang, Q., Zhu, G., & Wang, C. Y. (2025). Adsorption of phosphates on a novel eggshell Ca-modified anaerobic sludge-based biochar: Adsorption performance and mechanism. *Plos one*, *20(11),* Article 0337183. https://doi.org/10.1371/journal.pone.0337183
37. Ge, H., Huang, H., Xu, M., & Chen, Q. (2016). Cellulose/poly (ethylene imine) composites as efficient and reusable adsorbents for heavy metal ions. *Cellulose*, *23(4)*, 2527-2537. https://doi.org/10.1007/s10570-016-0973-3
38. Yu, S., Sun, C., Fang, S., Wang, C., Alharbi, N. S., & Chen, C. (2023). Preparation of cellulose@amidoxime by plasma-induced grafting technology and its potential application for uranium extraction. *Applied Surface Science*, *637*, Article 157883. https://doi.org/10.1016/j.apsusc.2023.157883
39. Isik, B., Ugraskan, V., Cakar, F., & Yazici, O. (2024). A comparative study on the adsorption of toxic cationic dyes by Judas tree (Cercis siliquastrum) seeds. *Biomass Conversion and Biorefinery*, *14(5)*, 6709-6723. https://doi.org/10.1007/s13399-022-02679-8
40. Zhang, L., Xue, W., & Gu, L. (2019). Modification of hyperbranched hemicellulose polymer and its application in adsorbing acid dyes. *Cellulose*, *26(9)*, 5583-5601. https://doi.org/10.1007/s10570-019-02483-0
41. Isik, B., Cakar, F., & Cankurtaran, O. (2023). Valorization of Urtica dioica roots as a highly-effective and eco-friendly biosorbent for adsorptive removal of hazardous textile dyes. *Materials Science and Engineering: B*, *293*,

Figures

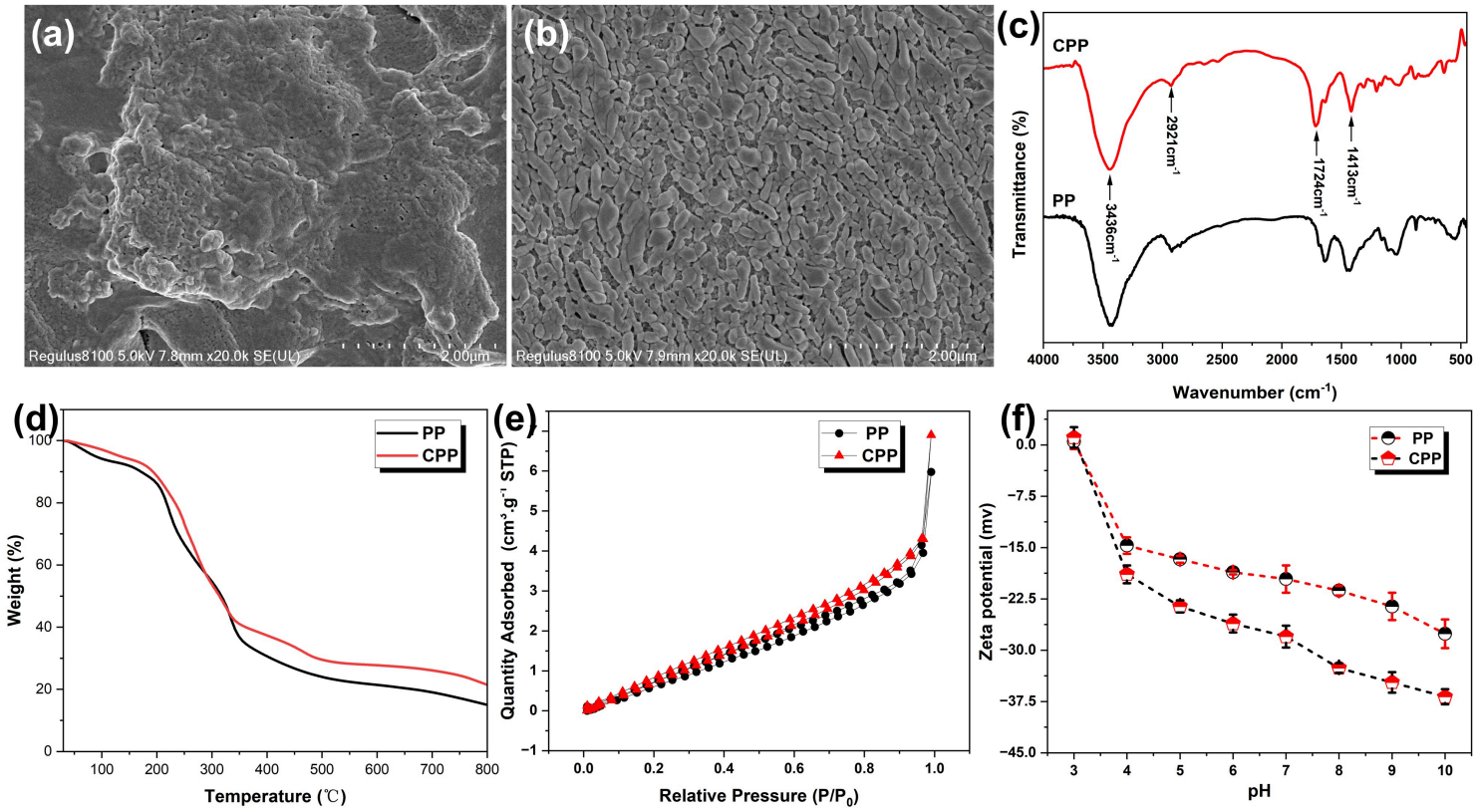


Figure 1

SEM images of CP (a) and CCP (b), FT-IR curve (c), TGA curve (d), N_2 adsorption-desorption curve (e), Zeta potential curve at different pH (f) of PP and CPP.

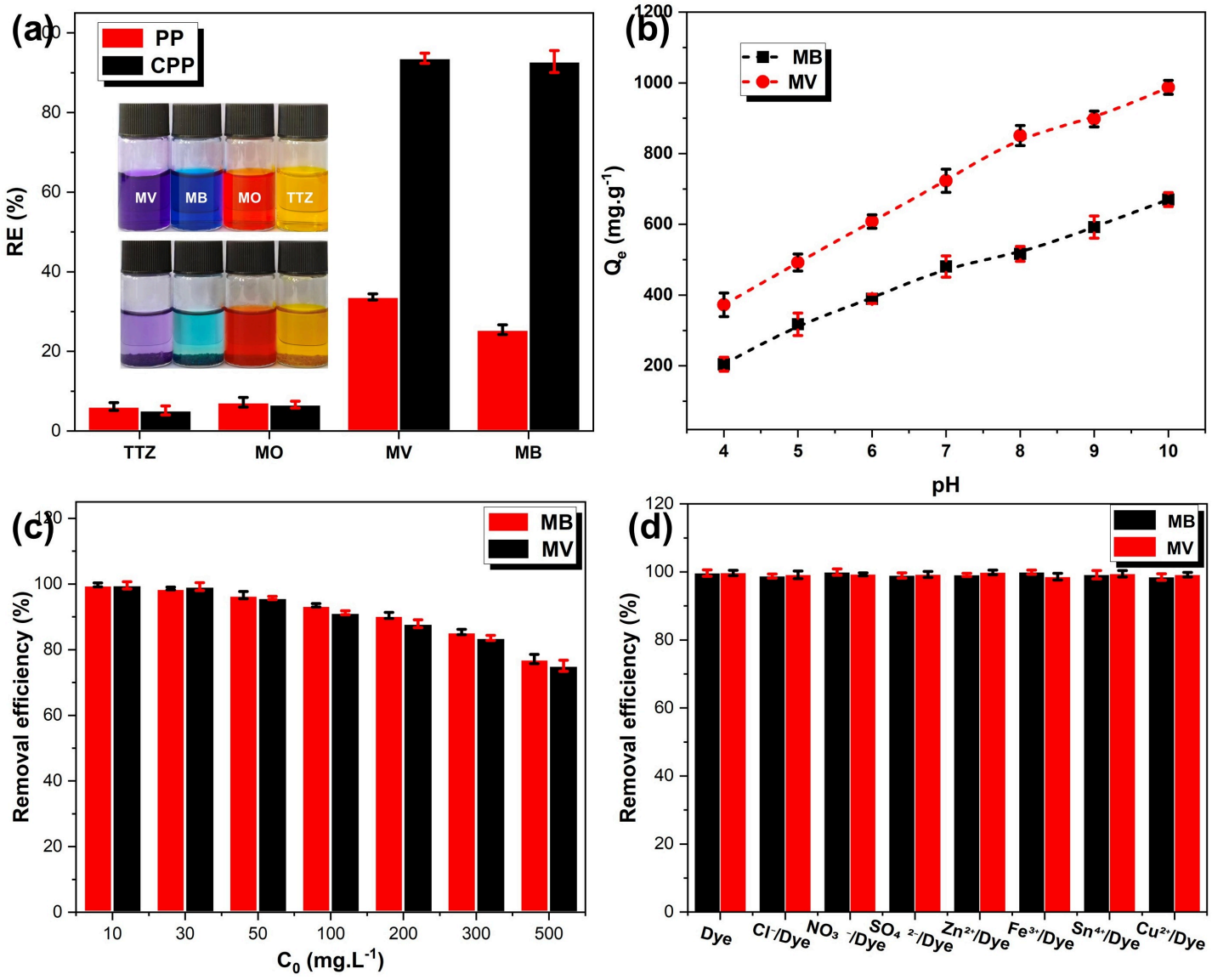


Figure 2

Removal efficiencies and visual removal performance of PP and CPP toward different dyes (a), adsorption capacities for MB and MV at different pH values (b), effects of initial dye concentration on the adsorption of MB and MV by CPP (c), and effects of coexisting ions (d).

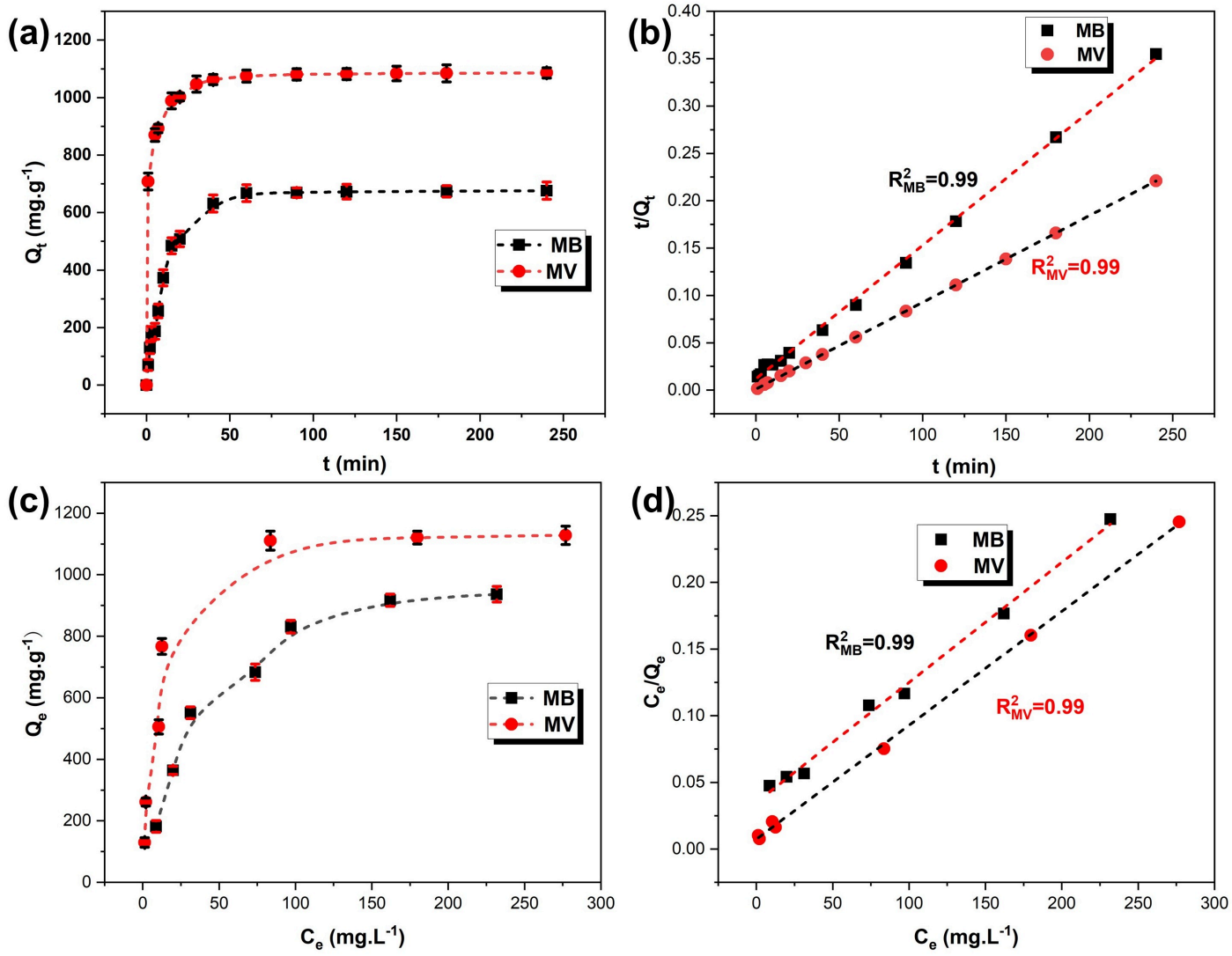


Figure 3

Effect of contact time on the adsorption of MB and MV by CCP (a), Pseudo-second-order kinetic model (b), adsorption isotherms of MB and MV on CCP (c) and Langmuir isotherm model (d).

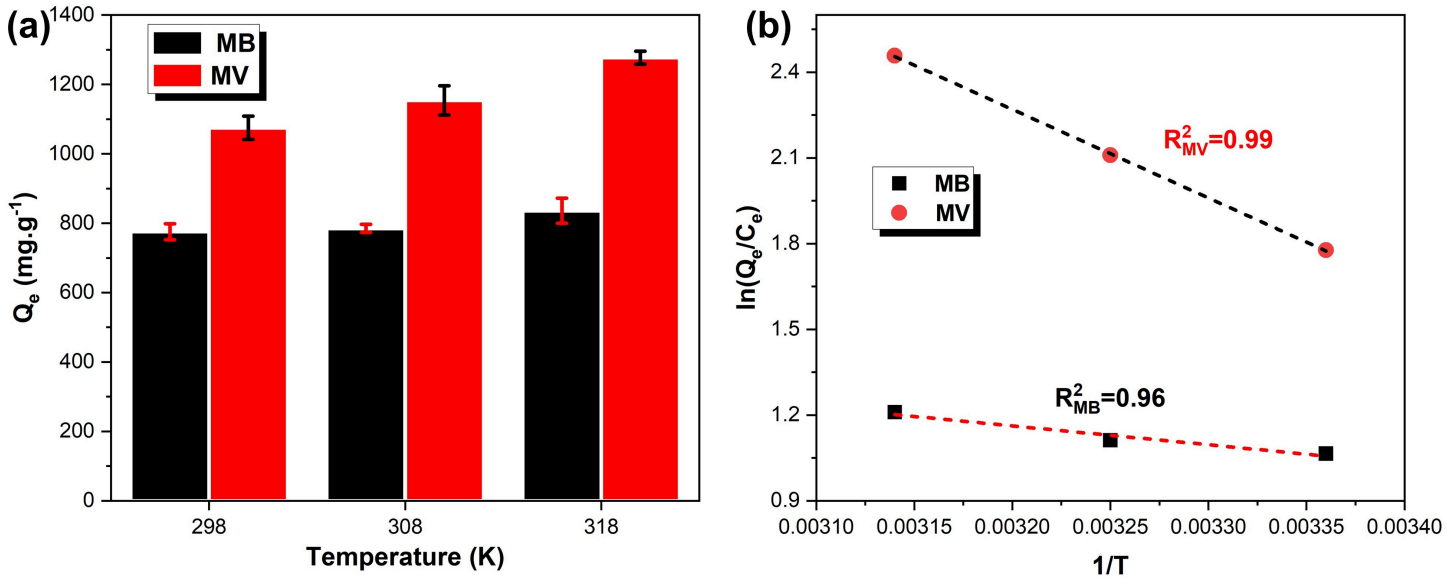


Figure 4

The adsorption capacity of CPP for MB and MV at different temperature(a), Plot of lnQ_e/C_e versus 1/T(b).

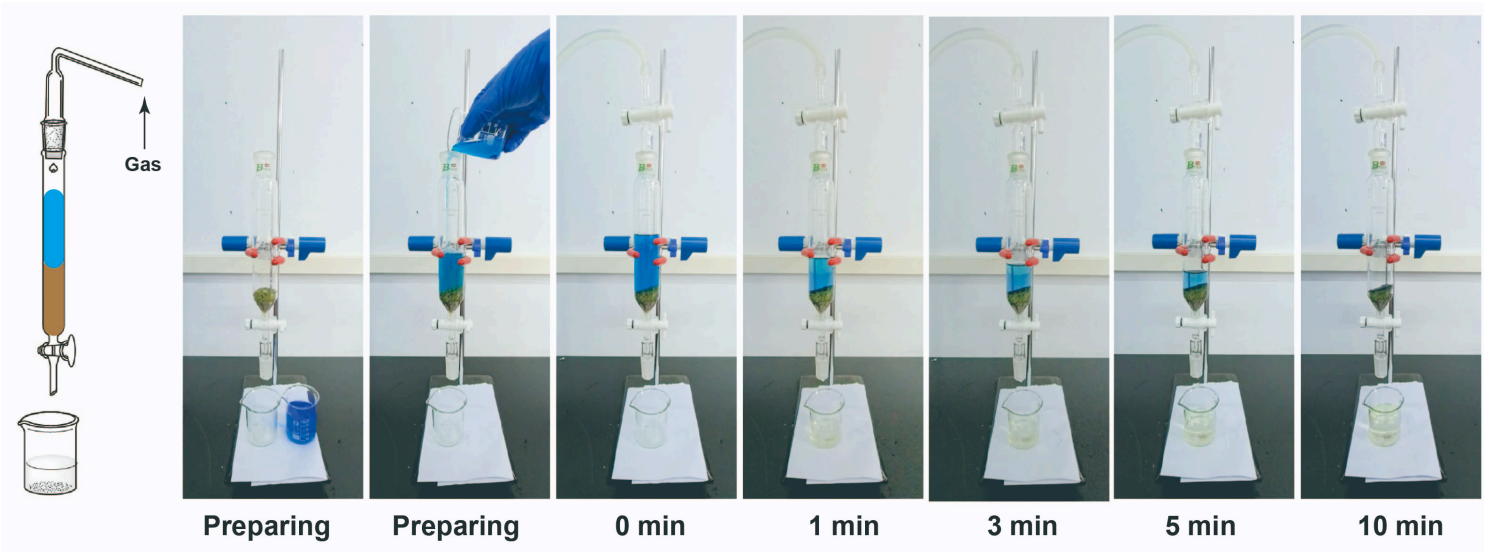


Figure 5

Video snapshots showing the MB solution passing through a rapidly packed CPP powder column (MB: 10 mg.L^{-1}).

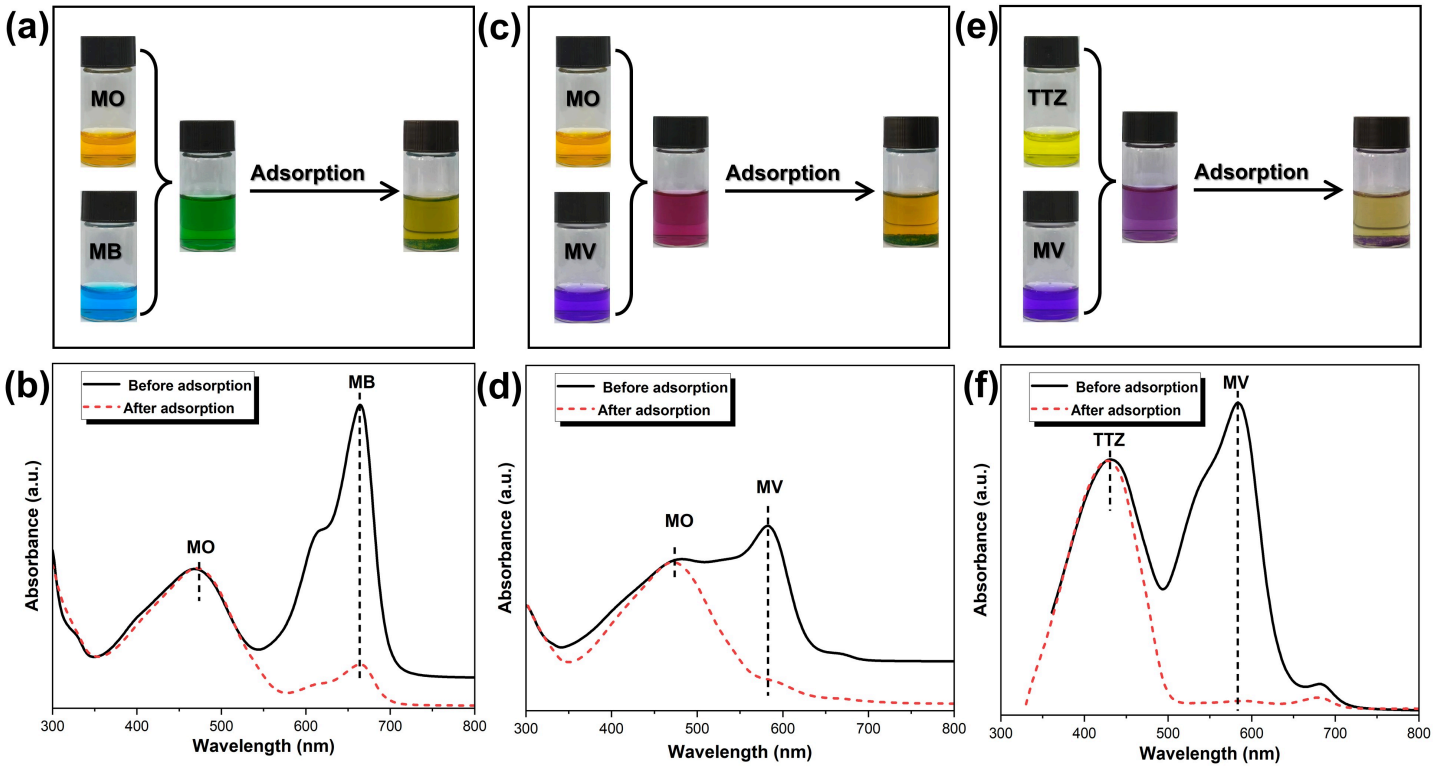


Figure 6

The photographs of MB/MO (a), MV/MO (c), MV/TTZ (e) mixed solutions before and after adsorption, and full-scan UV-vis spectra of MB/MO (b), MV/MO (d), MV/TTZ (f) systems before and after adsorption by CPP.

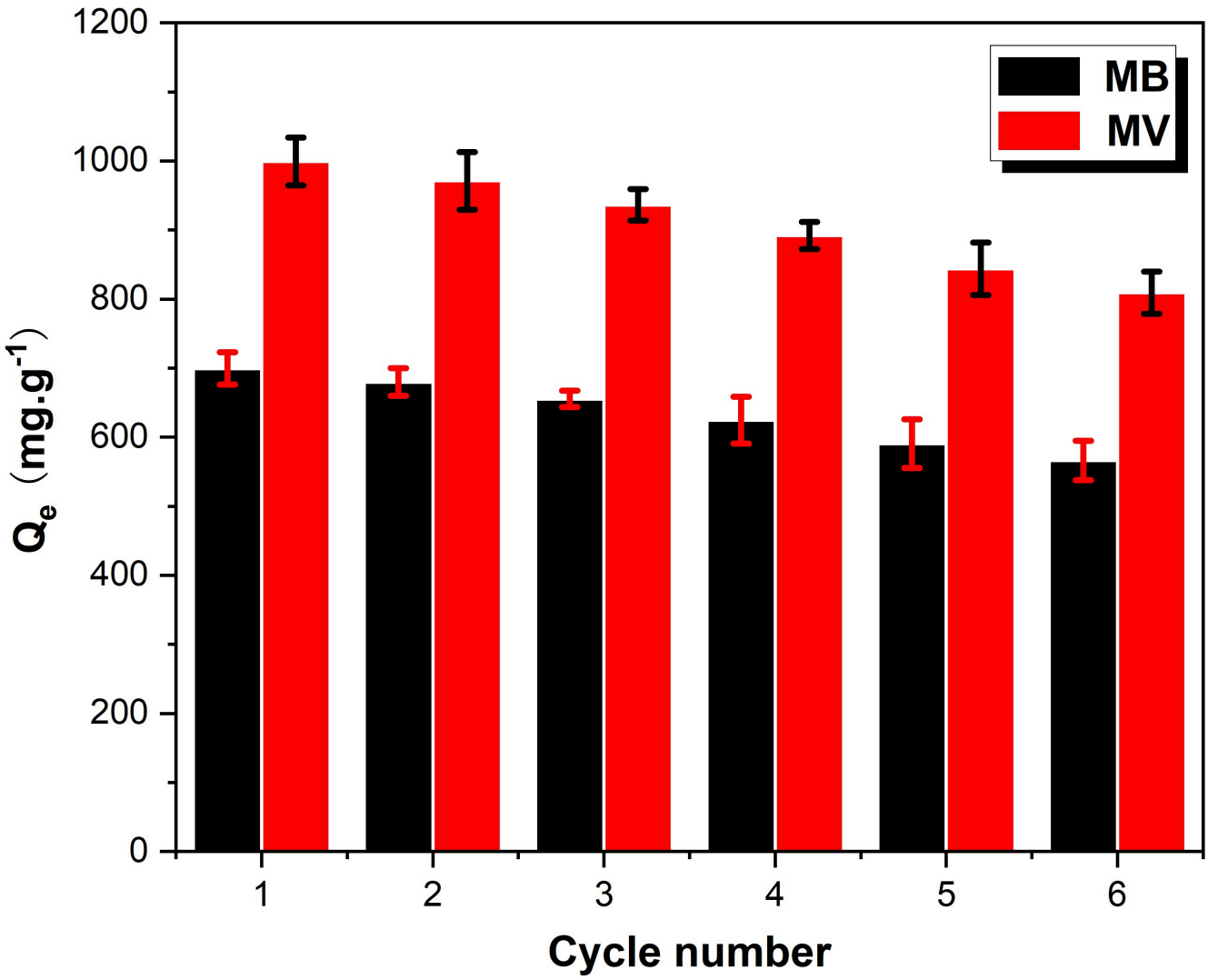


Figure 7

Removal rate of MB and MV by CPP after 6 consecutive adsorption-desorption cycles.

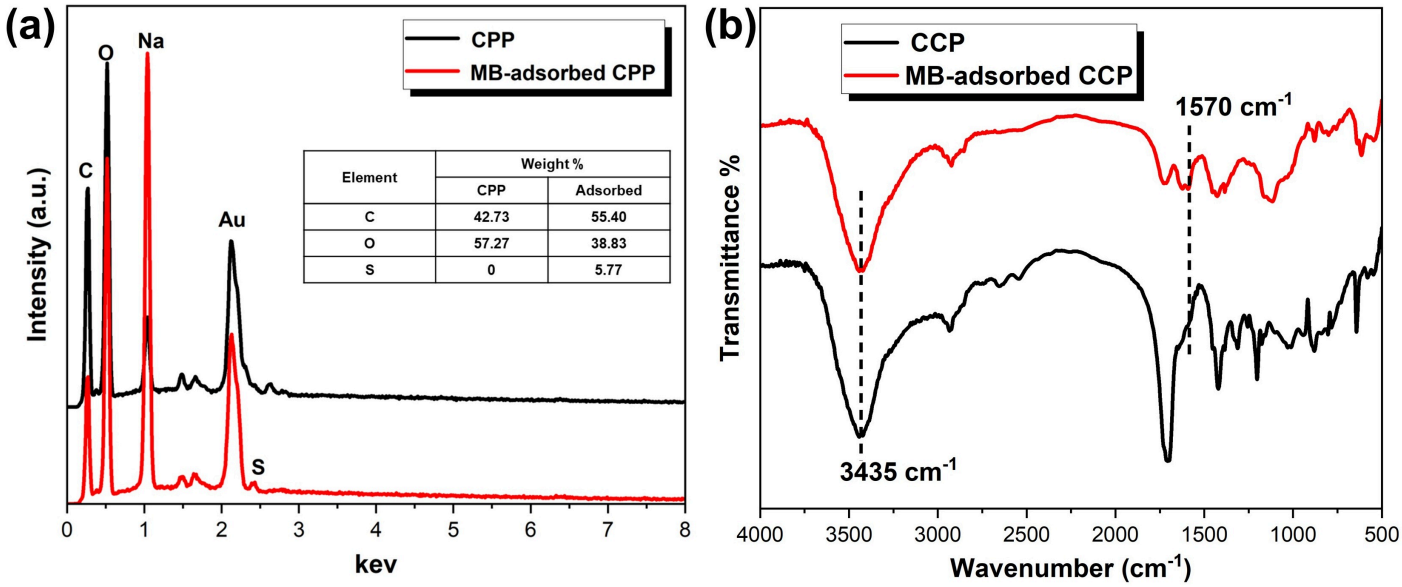


Figure 8

EDS curves (a) and FT-IR curves (b) of CPP before and after adsorbing MB.

Supplementary Files

This is a list of supplementary files associated with this preprint. Click to download.

- 20260618Supportinginformation.docx